

***Two-step continuous-flow synthesis of CuInSe<sub>2</sub> nanoparticles in a solar microreactor***

The Faculty of Oregon State University has made this article openly available.  
Please share how this access benefits you. Your story matters.

<b>Citation</b>	Kreider, P. B., Kim, K. J., & Chang, C. H. (2014). Two-step continuous-flow synthesis of CuInSe <sub>2</sub> nanoparticles in a solar microreactor. RSC Advances, 4(27), 13827-13830. doi:10.1039/C4RA00467A
<b>DOI</b>	10.1039/C4RA00467A
<b>Publisher</b>	Royal Society of Chemistry
<b>Version</b>	Accepted Manuscript
<b>Terms of Use</b>	<a href="http://cdss.library.oregonstate.edu/sa-termsfuse">http://cdss.library.oregonstate.edu/sa-termsfuse</a>

## COMMUNICATION

Two-Step Continuous-Flow Synthesis of CuInSe<sub>2</sub> Nanoparticles in a Solar Microreactor

Cite this: DOI: 10.1039/x0xx00000x

Peter B. Kreider, Ki-Joong Kim and Chih-Hung Chang\*

Received 00th January 2012,

Accepted 00th January 2012

DOI: 10.1039/x0xx00000x

www.rsc.org/

**A novel method of copper indium diselenide nanoparticle (CuInSe<sub>2</sub> NP) synthesis using a two-step, continuous flow, solar microreactor is reported here. This method allows for exceedingly fast heating and short reaction times using only radiative heat transfer from simulated, concentrated solar radiation. Chalcopyrite and sphalerite CuInSe<sub>2</sub> phases have both been synthesized by changing nucleation temperature and residence time through the solar microreactor, with higher nucleation temperatures and longer residence times allowing for the formation of the chalcopyrite CuInSe<sub>2</sub> phase.**

Copper indium diselenide (CuInSe<sub>2</sub>) semiconductor materials have been extensively studied as candidates for thin film absorber layers in high efficiency photovoltaic (PV) cells,<sup>1-3</sup> and to a much lesser extent as materials for other optical devices.<sup>4,5</sup> Chalcopyrite CuInSe<sub>2</sub> based PV devices are of particular interest because they have demonstrated long-term stability and the highest conversion efficiencies of all thin film based solar PV cells.<sup>6</sup> Most traditional CuInSe<sub>2</sub> thin film manufacturing practices suffer from poor energy efficiency and large carbon footprints brought on by poor material utilization, high processing temperatures, and the required use of vacuum systems.<sup>6,7</sup> For this reason, there has been a good deal of research work done on solution based synthesis of CuInSe<sub>2</sub> nanoparticle (NP) suspensions. These suspensions can be easily and inexpensively deposited or printed into thin film configurations at a fraction of the cost of traditional manufacturing techniques.<sup>8-11</sup> Most of the solution based processes are batch methods that require inert environments and relatively long synthesis times at high temperatures. The batch methods, while ideal for laboratory scale work, do not lend themselves well to larger scale production, which is necessary for successful commercialization. Here we report a novel synthetic method, a combination of a *continuous flow system*, a *micro-sized reactor*, and *solar energy*. The *continuous flow system* provides a convenient means to increase production rates to commercial scales; *micro-sized reactors* allow for finely tuned control of heat and mass

transfer properties, vastly reduced reaction times, and the ability to easily adjust reaction parameters; *solar energy* input, in this case from an artificial source, enables the possibility of a zero energy impact chemical manufacturing process for the production of nanoscale materials.

The continuous flow solar microreactor (CFSMR) system reported in this work (Fig. 1) starts with a coiled light absorber region which rapidly heats the precursor solution to temperatures high enough to start nucleation events. After this preliminary nucleation zone, there is a second light absorber which allows for continued particle growth at a secondary temperature. Continuous flow calorimetry using oleic acid as a test fluid confirmed 14.5 W of heat transfer to the fluid from the 20 W halogen bulb, yielding an overall heat transfer efficiency around 72.5 % (see notes and references for more detail).

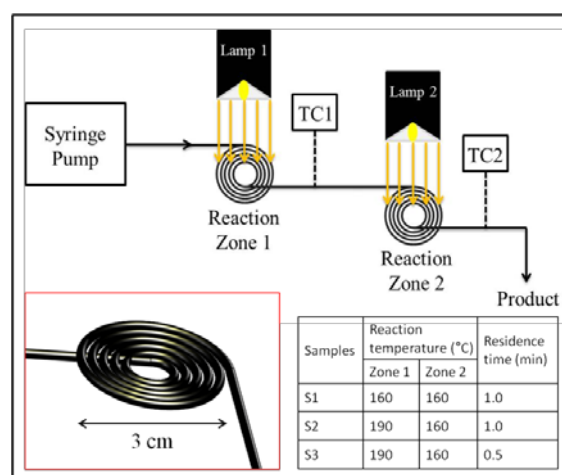


**Fig. 1** Schematic diagram of the CFSMR system. The inset in the lower left shows the enlarged image of coiled light absorber. The inset Table in the lower right shows the experimental conditions used in the CFSMR system.

Burst nucleation and controlled growth are the two critical steps towards the synthesis of uniform NPs. The hot-injection batch

synthesis method, where one precursor is injected into another already hot precursor, is the most commonly used process.<sup>8</sup> As a result of injection, the temperature drops and limits the growth rate of the newly formed nuclei. The CFSMR system was designed to take advantage of the rapid heating from concentrated radiation to facilitate burst nucleation in the first heating stage. A second heating stage then starts, which is designed to precisely control the growth of the already formed particle nuclei. In a typical  $\text{CuInSe}_2$  NP synthesis, a pre-mixed solution of  $\text{CuCl}$ ,  $\text{InCl}_3$ , and elemental Se in oleic acid and trioctylphosphine at room temperature was continuously pumped into the two-step solar microreactor heated by halogen lamps (see notes and references for more detail).

We investigated the particle sizes, morphologies, crystal structures, compositions, and optical properties of the synthesized  $\text{CuInSe}_2$  NPs using the CFSMR system. The field emission scanning electron microscope (FE-SEM) and corresponding transmission electron microscope (TEM) images of sample S1 show clusters of aggregated particles with irregular shape. In this case, nucleation and growth occur concurrently and thus the final product exhibit a broad (and undesirable) size distribution. It is therefore important to prevent additional nucleation events during the subsequent growth process by increasing the nucleation temperature. The morphologies of samples S2 and S3 synthesized at higher nucleation temperature are roughly spherical or spheroidal (Fig. 2A-2F). The synthesized  $\text{CuInSe}_2$  NPs range from 40 nm to 350 nm in diameter, and samples S2 and S3 had an average particle size of 219 nm and 143 nm, respectively (inset of Fig. 2B and 2C). The electron diffraction patterns are indicative of  $\text{CuInSe}_2$ , as shown in Fig. 2D-2F. During FE-SEM imaging, we collected the energy dispersive spectroscopy (EDS) spectra for three random locations on the sample. Compositions for the Cu/In/Se ratio were 1.00:0.93:2.18, 1.00:1.05:2.35, and 1.00:0.65:2.28 for samples S1, S2, and S3, respectively. Higher nucleation temperatures create conditions conducive to burst nucleation, leading to more uniform particle growth and lower size distributions. Longer residence times also allow the particles to grow and become stoichiometrically balanced  $\text{CuInSe}_2$ . S2 has a stoichiometric ratio close to  $\text{Cu/In/Se} = 1:1:2$ , while S3 shows an indium deficiency according to EDS results.

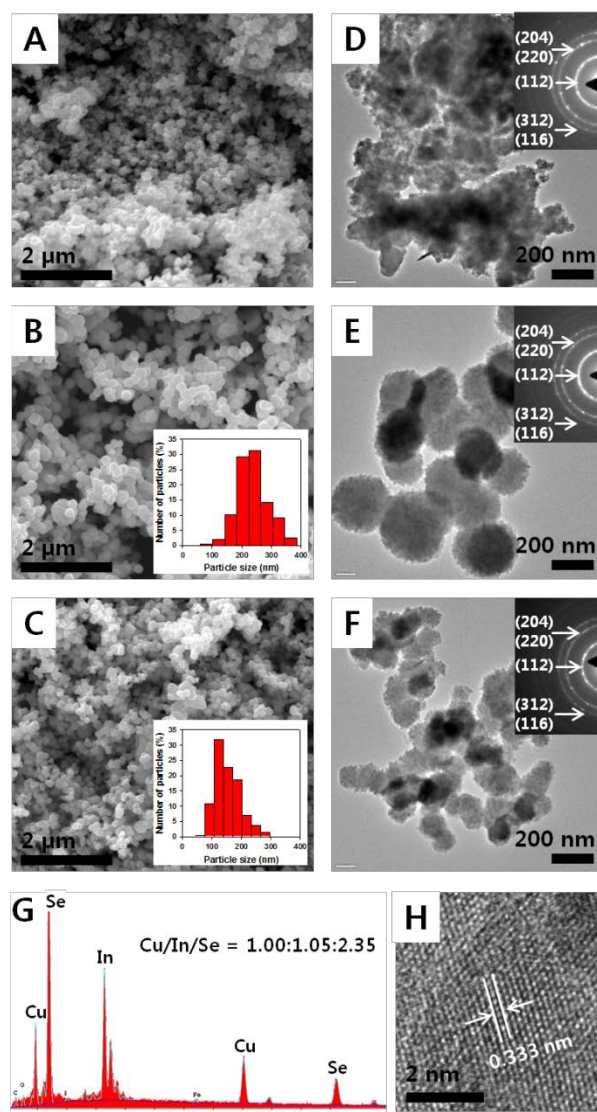


**Fig. 2.** FE-SEM images of samples (A) S1, (B) S2, and (C) S3 (inset of particle size distributions. The particle sizes were measured by counting at least 150 particles in the micrographs through ImageJ software). TEM images of samples (D) S1, (E) S2, and (F) S3 (inset of electron diffraction patterns). (G) EDS spectrum and (H) high-resolution TEM image of S2 synthesized in the CFSMR system.

The X-ray diffraction (XRD) patterns for all samples are very similar (Fig. 3A). The peaks correspond well with the JCPDS file No. 89-5646 for  $\text{CuInSe}_2$  with a body centered lattice structure. The peaks are located at  $2\theta = 26.7^\circ, 44.3^\circ, 52.4^\circ, 64.5^\circ,$  and  $71.0^\circ$ , respectively. These correspond to the (112), (204)/(220), (116)/(312), (400), and (316)/(332) planes of  $\text{CuInSe}_2$  and belong to the  $I-42d$  space group symmetry, which is in good agreement with the electron diffraction patterns in Fig. 2. There are several phases of  $\text{CuInSe}_2$  with nearly identical XRD patterns and some forms of copper selenide that share many similar peaks with  $\text{CuInSe}_2$ . There are no separate peaks observable for the typical intermediate products such as copper selenide and indium selenide, which indicates that the designed CFSMR system allows for very fast synthesis of  $\text{CuInSe}_2$  NPs within one minute.

Raman spectroscopy was also employed to further elicit information on the specific crystal structure of the synthesized CuInSe<sub>2</sub> NPs (Fig. 3B). The Raman peaks at 178–184 cm<sup>-1</sup> for all three samples confirms the presence of CuInSe<sub>2</sub> in either chalcopyrite and/or sphalerite phases. Characteristic peaks for each sample were fitted with Gaussian curves, as shown in Fig. 3B. S1 has a peak maximum at 184 cm<sup>-1</sup>, very close to the reported characteristic peak for sphalerite CuInSe<sub>2</sub>.<sup>12</sup> S2 has a Raman spectrum with a peak max at approximately 178 cm<sup>-1</sup>. Stoichiometric chalcopyrite CuInSe<sub>2</sub> usually has peaks ranging from 173 cm<sup>-1</sup> to 177 cm<sup>-1</sup>.<sup>12–14</sup> S3 shows a peak centered around 180 cm<sup>-1</sup>, which is likely also chalcopyrite structure. The slight blue shift for S3 is due to slight indium deficiency, which agrees well with the EDX results. Similar Raman spectra for CuInSe<sub>2</sub> NPs synthesized in batch reactions after reaction times of 24 h at elevated temperature have been reported,<sup>16</sup> whereas the spectra reported here are for particles synthesized in less than one minute.

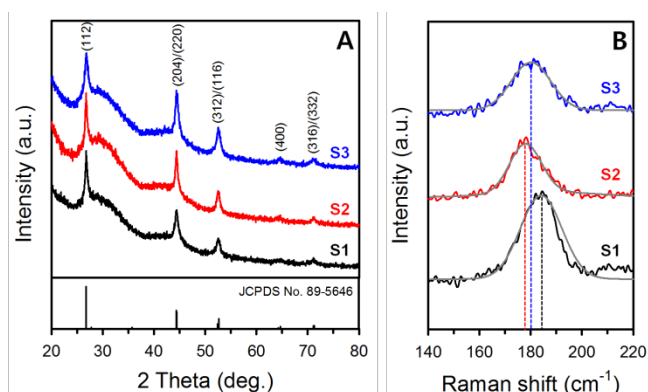


**Fig. 3.** (A) XRD patterns and (B) Raman spectra of the CuInSe<sub>2</sub> NPs synthesized via the CFSMR system. The XRD fingerprint of the JCPDS No. 89-5646 for CuInSe<sub>2</sub> is shown for reference. Raman spectra also show deconvolution curves from Gaussian fits, with peak maximums identified with dotted lines.

According to the literature, the sphalerite form of CuInSe<sub>2</sub> arises as a result of highly random distributions of Cu and In atoms in metal atom sites and that the transition to the chalcopyrite phase arises from ordered cation (Cu, In) arrangement in the sublattice.<sup>17</sup> The properties of S2 are indicative of the chalcopyrite phase of CuInSe<sub>2</sub>, which is desired as a potential candidate for thin film PV cells. Hereafter, we focus on the chalcopyrite phase and stoichiometrically balanced CuInSe<sub>2</sub> (S2). Fig. 2D shows the transmission electron microscopy (TEM) image of S2 where the particles seem to have adopted a flower-like configuration, which have been reported in the literature for the solvothermal synthesis of CuInSe<sub>2</sub> NPs previously.<sup>18–21</sup> The composition of S2 also showed a Cu/In/Se atomic ratio of 1.00:1.05:2.35, suggesting the desired stoichiometry of 1:1:2, according to EDS analysis (Fig. 2G). The orientation of the lattice structure in the high-resolution TEM image also shows a lattice spacing of 0.333 nm, corresponding to the (112) lattice plane of CuInSe<sub>2</sub> (Fig. 2H).

The absorption spectrum of S2 suspended in toluene was measured by ultra violet-visible absorbance spectroscopy (UV-Vis) (Fig. 4). The absorption maximum appears around 500 nm, which is in the center of the visible spectrum. A very similar spectrum is reported

in literature.<sup>22</sup> It is suggested that this broad absorption band around 500 nm is attributable to nonbonding copper *d* localized states.<sup>23</sup> The insert in Fig. 4 shows the linear extrapolation band-gap estimation method, yielding a value of 1.34 eV.

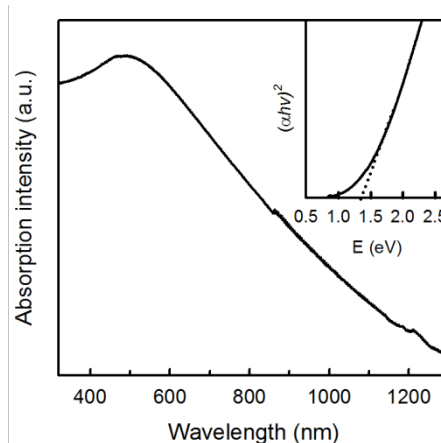


**Fig. 4.** UV-Vis absorption spectrum of S2 dispersed in toluene (Insert of the optical energy gap).

CuInSe<sub>2</sub> NPs of both chalcopyrite and sphalerite crystal structure were successfully synthesized in a novel CFSMR system with an initial nucleation zone followed by a growth zone. Stoichiometrically balanced Chalcopyrite CuInSe<sub>2</sub> NPs were grown at higher nucleation temperatures and longer residence times. The extremely simple reactor design allows for very rapid synthesis, with residence times less than one minute in length, which is at least an order of magnitude faster than traditional solvothermal synthesis methods. We believe this simple solar microreactor design could be easily employed for many different reaction chemistries.

This work was financially supported by the National Science Foundation's Process and Reaction Engineering Program under award CBET-1105061; matching grants from Oregon Nanoscience and Micro-technologies Institute (ONAMI) and Oregon Built Environment & Sustainable Technologies (BEST) center. We are thankful to Joshua Raznik at CAMCOR, University of Oregon, for his valuable assistance in obtaining, analyzing and interpreting high-resolution TEM data.

## Notes and references

Oregon Process Innovation Center, Microproducts Breakthrough Institute, School of Chemical, Biological & Environmental Engineering, Oregon State University, Corvallis, OR 97331, United States. Fax: +1 541 737 4600; Tel: +1 541 737 8548; E-mail: [chih-hung.chang@oregonstate.edu](mailto:chih-hung.chang@oregonstate.edu)

† Materials, synthesis, and characterization details: The precursors were prepared separately as follows. A solution of 0.11 M Copper (I) chloride (> 90 %, Alfa Aesar) and 0.33 M indium (III) chloride (99.99 %, Alfa Aesar) were added to a 4:1 mixture of oleic acid (OA, 70 %, Aldrich) and trioctylphosphine (TOP, 90 %, Aldrich), then stirred at 90 °C until all solids were dissolved completely and the solution turned a light yellow. Separately, 1.4 M selenium (99.5 %, Alfa Aesar) was added to TOP and stirred at 90 °C for 1 h until clear. The OA and TOP solvent system was based on a previous CuInSe<sub>2</sub> NPs solvothermal synthesis technique.<sup>24</sup> The prepared solutions were degasified under nitrogen flow for 30 min prior

to synthesis. No glove-box or Schlenk line were required for this synthetic procedure.

CuInSe<sub>2</sub> NPs were synthesized using a two-step solar microreactor system, as shown in Fig. 1. The reaction was carried out in a 1 m long (including connections) stainless steel tubing (o.d.: 1.6 mm, i.d.: 1.0 mm) wound into two separate coiled zones (3 cm diameter), which are irradiated by 20 W halogen lamps (740 series, Sunnex). The outer walls of the reactors were coated with high-temperature tolerant paint (2500 Flat Black, Pyromark) in order to increase absorption and conversion of incoming photons into thermal energy. The precursors were pre-mixed at a stoichiometric ratio of Cu/In/Se = 1:3:2 at room temperature. Here, the color of the mixed solutions did not change prior to heating, which indicates that each precursor did not prematurely react in the OA and TOP system. The pre-mixed solution was then pumped into the solar microreactor using a syringe pump (kd Scientific) at a flow rate of 1 or 2 mL min<sup>-1</sup>. Both reaction zone 1 and zone 2 were irradiated by a 20 W halogen lamp and the temperature was measured using K-type thermocouples inserted into the stream. The reaction temperatures were controlled by adjusting the distance of the lamps. The product was collected in a glass vial, and then ethanol was added to precipitate the CuInSe<sub>2</sub> NPs, followed by centrifugation at 5000 rpm for 10 min. The supernatant was discarded. The product was washed with toluene and ethanol was added to flocculate the CuInSe<sub>2</sub> NPs followed by an additional 5000 rpm for 10 min. The supernatant was again decanted, and the final product was re-dispersed in toluene or dried under nitrogen for further characterization.

Calorimetry experiments were performed after the high temperature paint was applied to the receiver zones. Each lamp uses 20 W of power and the OA calorimetric test fluid absorbed almost 14.5 W of energy. The energy transfer efficiency from the heat produced by the lamps to heat liquid inside the coils about 72.5 %. The equation used to calculate efficiency ( $\eta$ ) is as follows,  $\eta = \dot{m} \cdot C_p \cdot \Delta T \cdot P^{-1}$ , where  $\dot{m}$  is the mass flow rate,  $C_p$  is the heat capacity of OA,  $\Delta T$  is the temperature change from inlet to outlet, and  $P$  is the power consumed by the halogen lamp, respectively.

FE-SEM analysis was conducted by FEI Quanta 600 using 15 kV accelerating voltage. EDS data was collected using the Genesis Apex System attached to the FE-SEM. XRD patterns were obtained using a Bruker D8 Discover instrument operating at 40 kV and a current of 40 mA with Cu K $\alpha$  radiation (0.154 nm) in the  $2\theta$  scan range from 20° to 80° with a step size of 0.05°. The measured XRD patterns were compared with JCPDS files. Raman spectra were recorded using a Horiba LabRAM HR 800 with an Ar ion laser (532.06 nm) and a CCD detector. Raman peaks were calibrated using a silicon wafer. HRTEM was performed by an FEI Titan FEG-TEM at an accelerating voltage of 200 kV. UV-Vis absorption spectra were measured using a Jasco V-670 UV-Vis-NIR spectrophotometer in the range of 300-1300 nm. The band gap was estimated by extrapolating the linear region of a plot of the squared absorbance versus the photon energy.

1. W. N. Shafarman, S. Siebentritt and L. Stolt, Handbook of Photovoltaic Science and Engineering, ed. A. Luque and S. Hegedus, Wiley, New York, 2nd edn., 2011, ch. 13, pp. 546-599.
2. Q. Guo, S. J. Kim, M. Kar, W. N. Shafarman, R. W. Birkmire, E. A. Stach, R. Agrawal and H. W. Hillhouse, Nano Lett., 2008, 8, 2982-2987.

3. W. Su, C. Wu, I. Cheng, Organic, Inorganic and Hybrid Solar Cells: Principles and Practice, John Wiley & Sons, 2012
4. J. J. Wang, Y. Q. Wang, F. F. Cao, Y. G. Guo and L. J. Wan, J. Am. Chem. Soc., 2010, 132, 12218-12221.
5. P. M. Allen and M. G. Bawendi, J. Am. Chem. Soc., 2008, 130, 9240-9241.
6. M. Kemell, M. Ritala and M. Leskelä, Crit. Rev. Solid State Mater. Sci., 2005, 30, 1-31.
7. C. J. Hibberd, E. Chassaing, W. Liu, D. B. Mitzi, D. Lincot and A. N. Tiwari, Prog. Photovoltaics, 2010, 18, 434-452.
8. H. W. Hillhouse and M. C. Beard, Curr. Opin. Colloid Interface Sci., 2009, 14, 245-259.
9. S. E. Habas, H. A. S. Platt, M. F. A. M. van Hest and D. S. Ginley, Chem. Rev., 2010, 110, 6571.
10. C. Wen, X. Weidong, W. Juanjuan, W. Xiaoming, Z. Jiasong and L. Lijun, Mater. Lett., 2009, 63, 2495-2498.
11. S. Peng, J. Liang, L. Zhang, Y. Shi and J. Chen, J. Cryst. Growth, 2007, 305, 99-103.
12. S. Shirakata, H. Kubo, C. Hamaguchi and S. Isomura, Jpn. J. Appl. Phys., 1997, 36, 1394-1396.
13. O. Ramdani, J. Guillemoles, D. Lincot, P. Grand, E. Chassaing, O. Kerrec and E. Rzepka, Thin Solid Films, 2007, 515, 5909-5912.
14. J. Alvarez-García, E. Rudigier, N. Rega, B. Barcones, R. Scheer, A. Pérez-Rodríguez, A. Romano-Rodríguez, J. Morante, Thin Solid Films, 2003, 431, 122-125.
15. M. Valdés, M. Vázquez, J Solid State Electrochem., 2012, 16, 3825-3835
16. C. L. Exstrom, S. A. Darveau, A. L. Martinez-Skinner, M. Ingersoll, J. Olejnicek, A. Mirasano, A. T. Haussler, J. Huguenin-Love, C. Kamler and M. Diaz, Proceedings of the 33th IEEE Photovoltaic Specialists Conference, IEEE, San Diego, 2008.
17. H. Liu, Z. Jin, W. Wang and J. Li, Cryst. Eng. Comm., 2011, 13, 7198-7201.
18. J. Y. Chang, M. H. Tsai, K. L. Ou, C. H. Yang and J. C. Fan, Cryst. Eng. Comm., 2011, 13, 4236-4243.
19. S. L. Castro, S. G. Bailey, R. P. Raffaele, K. K. Banger and A. F. Hepp, Chem. Mater., 2003, 15, 3142-3147.
20. M. A. Malik, P. O'Brien and N. Revaprasadu, Adv. Mater., 1999, 11, 1441-1444.
21. C. H. Chang and J. M. Ting, Thin Solid Films, 2009, 517, 4174-4178.
22. J. Xu, C. Y. Luan, Y. B. Tang, X. Chen, J. A. Zapien, W. J. Zhang, H. L. Kwong, X. M. Meng, S. T. Lee and C. S. Lee, ACS Nano, 2010, 4, 6064-6070.
23. J. Xiao, Y. Xie, Y. Xiong, R. Tang and Y. Qian, J. Mater. Chem., 2001, 11, 1417-1420.
24. H. D. Jin and C. H. Chang, J. Nanopart. Res., 2012, 14, 1180.